Theoretical Study of the Mechanism of NO_2 Production from NO + ClO

Hasan Sayin and Michael L. McKee*

Department of Chemistry and Biochemistry, Auburn University, Auburn, Alabama 36849

Received: February 8, 2005; In Final Form: March 15, 2005

The reaction of NO with ClO has been studied theoretically using density-functional and wave function methods (B3LYP and CCSD(T)). Although a barrier for cis and trans additions could be located at the RCCSD(T) and UCCSD(T) levels, no barrier exists at the B3LYP/6-311+G(d) level. Variational transition state theory on a CASPT2(12,12)/ANO-L//B3LYP/6-311+G(d) surface was used to calculate the rate constants for addition. The rate constant for cis addition was faster than that for trans addition (cis:trans 1:0.76 at 298 K). The rate constant data summed for cis and trans addition in the range 200−1000 K were fit to a temperature-dependent rate in the form $k_{dis} = 3.30 \times 10^{-13} T^{0.558} \exp(305/T)$ cm^3·molecule^{-1}·s^{-1}, which is in good agreement with experiment. When the data are fit to an Arrhenius plot in the range 200−400 K, an activation barrier of −0.35 kcal/mol is obtained. The formation of $ClNO_2$ from ONOCl has a much higher activation enthalpy from the trans isomer compared to the cis isomer. In fact, the preferred decomposition pathway from *trans*-ONOCl to NO_2 + Cl is predicted to go through the *cis*-ONOCl intermediate. The trans → cis isomerization rate constant is $k_{iso} = 1.92 \times 10^{13} \exp(-4730/T)$ s^{-1} using transition state theory.

Introduction

The concentrations and chemistry of the ClO_x and NO_x radicals are important for understanding global atmospheric chemistry.[1] The ClO_x and NO_x radicals are involved in tropospheric ozone production and stratospheric ozone loss.[2,3] Generally, chlorine (Cl) is oxidized by ozone in the stratosphere and forms ClO, which can be removed by other reactions. Nitrogen oxides (NO_x) act as sinks for ClO, which are transformed into temporary reservoir species, such as $ClONO_2$ and HCl. These reservoir species do not react with ozone and are slowly removed from the stratosphere.

Although there have been many studies on atmospheric chlorine chemistry, there are still discrepancies concerning the atmospheric chlorine budget.[4,5] Specifically, there is a missing reservoir of inorganic chlorine in the stratosphere that may not be accounted for by $ClONO_2$ and HCl alone. For example, it is possible that nitryl chloride ($ClNO_2$) could also be an important chlorine reservoir.[6] Photolysis of $ClNO_2$ is predicted to be rapid in sunlight and may be the dominant loss mechanism, yielding primarily atomic chlorine.[7]

The recombination of ClO and NO radicals is known to produce NO_2 and Cl radicals[8−13] (eqs 1−4) through possible involvement of ONOCl and/or $ClNO_2$ as intermediates.

$$ClO + NO \rightarrow ONOCl \quad (1)$$

$$ONOCl \rightarrow Cl + NO_2 \quad (2)$$

$$ONOCl \rightarrow ClNO_2 \quad (3)$$

$$ClNO_2 \rightarrow Cl + NO_2 \quad (4)$$

Experimental studies on the NO and ClO reaction between 200 and 400 K[9,10,13] have shown the reaction to have a negative activation barrier. Although the pressure dependence of the reaction has not been reported, the concentration of the bath gas in the Leu et al. study[10] was much higher than the concentration of the reactants, which may suggest that their results may be near the high-pressure limit. Several studies[8,11,12] report rate constants at only one temperature (298 K), and these results are in agreement with the temperature-dependence experimental results.[9,10,13]

The ONOX (X = OH, F, Cl) potential energy surfaces are expected to share some similarity.[14−18] When X = OH, the concerted formation of HNO_3 from HOONO is still very much in doubt.[14,17,18] Zhao et al.[14] showed that there is no direct isomerization between HOONO and $HONO_2$. They explained the mechanism of O−O cleavage from *cis*-HOONO to the formation of NO_2 + OH and calculated a 18−19 kcal/mol activation barrier for this process. On the other hand, when X = F, Ellison et al.[15] showed that ONOF forms FNO_2 on a continuously connected PES through a transition state with an activation barrier of 22 ± 3 kcal/mol. Zhu and Lin[16] recently calculated an isomerization path between *cis*-ONOCl and $ClNO_2$ with an activation barrier of 21.2 kcal/mol (through NO_2 + Cl).

In the following study, we will use electronic-structure methods to calculate the potential energy surface for the formation of NO_2 + Cl from NO + ClO. We will calculate the rate constant for disappearance of reactants (k_{dis}) as well as the rate constant for formation of products (k_{obs}) over the temperature range 200−1000 K. At the temperatures and pressures used in the experimental studies, it is not known whether the dependence of the rate constant on temperature is in the falloff or pressure-independent regime. Because the concentration of bath gas is much larger than the concentration of reactants, the reaction may be close to pressure independent. All the calculated rate constants reported below are at the high-pressure limit.

Computational Method

Because B3LYP density functional theory (DFT) has been shown to give reasonable structures and vibrational frequencies for halogen compounds,[19−22] we decided to use that method to calculate the PES. However, to check the DFT results, we also decided to use a more accurate method to determine the minima, transition states, and thermodynamic properties.

10.1021/jp050695w CCC: $30.25
Published on Web 05/06/2005

TABLE 1: Relative Energies[a] (kcal/mol) at the B3LYP/6-311+G(d), G3B3, and CCSD(T)/cc-pVTZ//CCSD(T)/cc-pVDZ Levels for Various Species Involved in the NO + ClO Reaction

	ΔH (0 K)			ΔH (298 K)			ΔG (298 K)		
	B3LYP	G3B3	CCSD(T)/cc-pVTZ	B3LYP	G3B3	CCSD(T)/cc-pVTZ[b]	B3LYP	G3B3	CCSD(T)/cc-PVTZ
NO + ClO	0.00	0.00	0.00	0.00	0.00	0.00	0.00	0.00	0.00
t-ONOCl	−27.08	−31.10	−27.37	−27.94	−31.94	−28.21 (−28.3)	−18.03	−22.02	−18.28
c-ONOCl	−31.07	−32.78	−30.34	−32.06	−33.75	−31.34 (−31.3)	−21.99	−23.68	−21.15
ONOCl-ts	−16.71	−21.99	−18.31	−17.85	−23.12	−19.46 (−19.3)	−7.61	−12.88	−9.12
ON−OCl-ts-c			−3.86			−4.31			3.94
ON−OCl-ts-t			−3.17			−3.49			3.76
ON−OCl-ts-c[c]			5.94			5.36			14.00
ON−OCl-ts-t[c]			8.10			7.49			16.43
NO_2Cl-ts	−18.84	−21.66	−17.20	−20.16	−22.96	−18.45 (−18.0)	−9.66	−12.46	−7.64
Abst-Cl-ts-t	−3.88	10.71	4.54	−4.88	9.71	3.62	5.23	19.82	13.56
Abst-Cl-ts-c			−10.75			−11.59			−2.93
Cl-add-NO_2-ts	−16.29	−12.17	−10.17	−16.92	−12.77	−11.01	−11.46	−2.53	−1.85
Cl-add-NO_2-ts[c]			−13.62			−15.77			−6.60
NO_2 + Cl	−15.49	−10.12	−10.14	−15.79	−10.40	−10.42 (−10.1)	−13.79	−8.41	−8.86
$ClNO_2$	−46.01	−44.85	−41.04	−47.34	−46.13	−42.30 (−42.2)	−36.34	−35.13	−31.32

[a] The spin−orbit correction (SOC) of NO (ref 31), ClO (ref 32), and Cl (ref 33) are included in the G3B3 and CCSD(T)/cc-pVTZ levels. [b] The values in parentheses are taken from ref 16. [c] Geometries are optimized at the UCCSD(T)/cc-pVDZ level.

Because the CCSD(T) method (with a reasonable basis set) yields very good results for difficult chemical systems such as O_3 and FOOF species,[23,24] we used it (with finite-difference derivatives) to optimize all of the stationary points on the PES.

All electronic structure calculations have used the Gaussian03[25] and Molcas6[26] program systems. Optimization and frequency calculations for the NO + ClO potential energy surface were carried out at the B3LYP/6-311+G(d) and CCSD(T) levels (Figures 1 and 2). All imaginary frequencies for transition states were animated by using the graphical program MolDen[27] to make sure that the motion was appropriate for converting reactants to products.

In transition states involving bond formation or bond breaking, a lower-energy spin broken-symmetry solution was obtained at the UDFT or UHF levels. For DFT calculations, we used the spin broken-symmetry results. However, for the CCSD(T) calculations, it was not clear whether the spin-restricted (RCCSD(T)) or spin-unrestricted (UCCSD(T)) method would produce more reliable results. In the work by Ellison et al.[15] on the ONOF → FNO_2 transition state a variety of post-SCF methods were used. At the RCCSD(T)/DZP and RCCSD(T)/pVTZ levels, the activation energies were 3 and 4 kcal/mol lower than those at the UCCSD(T)/DZP and UCCSD(T)/pVTZ levels, respectively, and in better agreement with their best computational results. Thus, although the UHF reference state is lower in energy than the RHF for these transition states, it appears that the RHF reference may be a better choice as the reference function for the post-SCF perturbative expansion.

Our RCCSD(T) and UCCSD(T) results for the NO + ClO reactions exhibit the same behavior, but more extreme. With respect to separated NO + ClO radicals computed at the UCCSD(T) level, the activation barriers for cis and trans addition were 5.36 and 7.49 kcal/mol, respectively. This result is in contrast to the B3LYP/6-311+G(d) results, where no transition state could be located, as well as CASPT2 results on fixed ON−OCl geometries, where the energy decreased monotonically as the N−O distance decreased. The RCCSD(T) method located transition states for cis and trans addition that were 4.31 and 3.49 kcal/mol *below* NO + ClO. Thus, the RCCSD(T) potential energy surface has a maximum for the formation of the N−O bond, but the stability of the entire surface at these large N−O distances is overestimated because it is below the energy of the reactants (NO + ClO).

The CCSD(T) optimizations and frequency calculations were carried out with the correlation-consistent cc-pVDZ basis of Dunning[28] with single-point calculations using the cc-pVTZ basis set[29] (i.e., CCSD(T)/cc-pVTZ//CCSD(T)/cc-pVDZ). The G3B3 method[30] was used with manual assembly of the components where we used B3LYP/6-311+G(d) optimized geometries and unscaled vibrational frequencies with all other calculations and corrections at standard levels. For transition states which were lower in energy using the UDFT spin broken-symmetry approach, the corresponding G3B3 calculations (including the post-SCF steps) were based on the spin broken-symmetry UHF wave function. The first-order spin−orbit corrections are included for NO,[31] ClO,[32] and Cl[33] (0.11, 0.30, and 0.78 kcal/mol, respectively) in all of the relative energy comparisons in Table 1.[34]

The reaction coordinate for the cis and trans approach of NO and ClO was constructed by optimizing the structure with spin broken-symmetry UDFT while fixing the N···O distance between the two radicals. In this way, a set of structures, where the N···O distance was fixed to 4.00, 3.75, 3.50, 3.25, and 3.00 Å, was obtained. Harmonic vibrational frequencies were computed for each structure along the cis and trans reaction coordinate. At each structure, one imaginary frequency was obtained, corresponding to the N···O stretch. The only exception was at a 4.00 Å separation along the trans reaction coordinate which was not used in the subsequent rate calculations.

The large difference between the UCCSD(T) and RCCSD(T) energies for the transition states of the NO + ClO addition reactions indicates that electron correlation methods based on a single reference are not appropriate for this part of the potential energy surface. For that reason, single-point calculations were made with a 12-electron 12-orbital complete active space[35] (CAS(12,12)) and the ANO-L basis set[36] with dynamic electron correlation introduced at the MP2 level (CASPT2).[37] At each structure, four singlet electronic states were computed, two $^1A'$ states and two $^1A''$ states. Both radicals, NO and ClO, have $^2\Pi$ ground states. As the two radicals approach, the electronic and spatial degeneracy will be lifted to give rise to a total of sixteen microstates, four singlet states, and four triplet states. The "reactive" state will correspond to $^1A'$ where the unpaired electron on each radical approaches in the reaction plane. The other electronic states will be occupied according to the Boltzmann distribution. We computed the

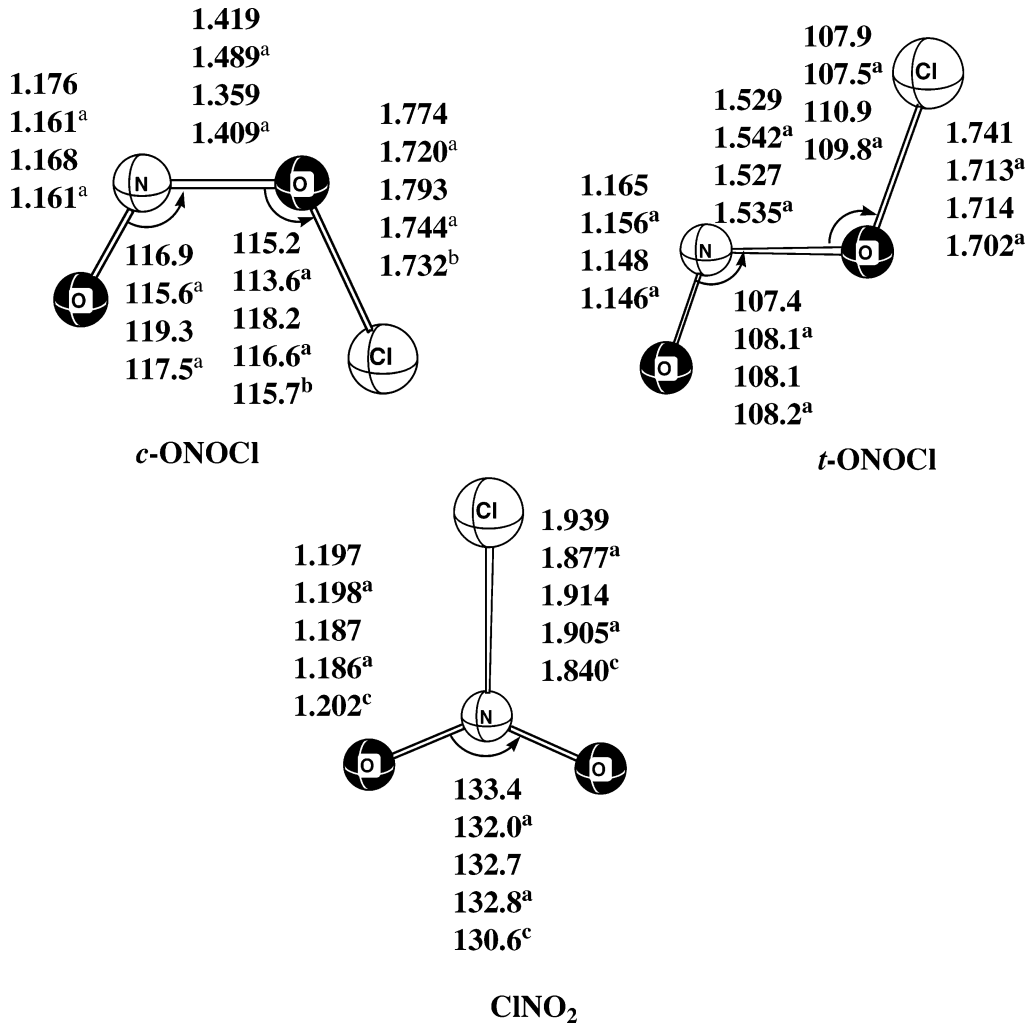

Figure 1. Optimized geometry of *cis*-,*trans*-ONOCl and $ClNO_2$ isomers. Bond lengths are in angstroms and angles are in degrees. Data in the first row and third row are calculated at the CCSD(T)/cc-pVDZ and B3LYP/6-311+G(d) levels, respectively. Calculated values[a] at the CCSD(T)/TZ2P (second row) and B3LYP/TZ2P (fourth row) levels, respectively, are taken from ref 19. Experimental values[b,c] are taken from refs 42 and 52, respectively.

electronic partition function to determine the fraction of reactive encounters which are in the "reactive" electronic state. At a short N···O separation where the "reactive" electronic state is already stabilized, the fraction is 0.98 at 200 K and 0.54 at 1000 K (3.00 Å, cis addition). At 4.00 Å the fraction is 0.36 at 200 K and 0.27 at 1000 K (cis addition). Because we are only considering the four close-lying singlet states, complete degeneracy would result in a 0.25 factor for each state.

Rate constants for the NO + ClO → NO_2 + Cl reaction were calculated with Polyrate-9.3[38] and VariFlex-1.0.[39] Rate constants were computed at each N−O separation (4.00, 3.75, 3.50, 3.25, and 3.00 Å) as a function of temperature (Table S4). For the cis approach, the smallest rate constant was found at 4.0 Å at each temperature. Technical difficulties prevented us from calculating rate constants at longer N−O separations. For the trans approach, the smallest rate constant was obtained at a N−O separation of 3.50 Å.

Because the formation of NO + ClO occurs without a barrier on the potential energy surface, we used VariFlex, a program designed for this task, to calculate the rate constants for cis and trans addition. VariFlex is a variational RRKM code that solves the master equation involving multistep vibrational energy transfer for the excited intermediate ONOCl. The enthalpy barrier for trans → cis isomerization of ONOCl is 8.75 kcal/mol (11.88 kcal/mol reverse barrier). We calculated rate constants with ChemRate[40] with harmonic frequencies at B3LYP/6-311+G(d) and energies at CCSD(T)/cc-pVTZ//CCSD(T)/cc-pVDZ. For calculations using Polyrate, we used B3LYP/6-311+G(d) for the IRC and harmonic frequencies and G3B3//B3LYP/6-311+G(d) for energies.

Results and Discussion

It is widely accepted that the reaction NO + ClO → NO_2 + Cl involves the ONOCl intermediate, which has two distinct conformers, *cis*- and *trans*-ONOCl, as well as the $ClNO_2$ isomer for which there exists reliable experimental data (Figure 3). However, there are few reliable experimental data available for the other ONOCl compounds. Because there is no evidence for OClNO,[41] we did not include this isomer in our study. The equilibrium structure for *cis*-ONOCl (Figure 1) is consistent with the earlier studies and experimental results.[19,42]

Figure 1 shows that the Cl−N bond distance of $ClNO_2$ has the largest sensitivity with respect to the method, with CCSD(T)/cc-pVDZ giving the longest Cl−N bond distance and CCSD(T)/TZ2P the shortest. Experimentally,[43] the enthalpy of the reaction NO + OCl → $ClNO_2$ is −42.87 kcal/mol, which is almost same as the CCSD(T)/cc-pVTZ//CCSD(T)/cc-pVDZ result of −42.30 kcal/mol. The experimental[43] enthalpy difference between *cis*-ONOCl and reactants (NO + ClO) is

TABLE 2: Harmonic Frequencies of *trans*-ONOCl, *cis*-ONOCl, and $ClNO_2$ in cm^{-1}

method	$\omega_1(a')$	$\omega_2(a')$	$\omega_3(a')$	$\omega_4(a')$	$\omega_5(a')$	$\omega_6(a'')$
			t-ONOCl			
B3LYP/TZ2P[a]	1834	879	660	404	259	178
B3LYP/6-311+G(d)	1854	874	645	403	255	182
CCSD(T)/TZ2P[a]	1754	855	607	407	212	170
CCSD(T)/cc-pVDZ	1800	852	646	403	263	173
			c-ONOCl			
B3LYP/TZ2P[a]	1741	868	647	365	229	398
B3LYP/6-311+G(d)	1732	868	673	363	212	426
CCSD(T)/TZ2P[a]	1715	850	638	416	249	341
CCSD(T)/cc-pVDZ	1731	859	618	430	245	378
expt[b]	1715	858	644	406	260−280	344
			$ClNO_2$			
B3LYP/TZ2P[a]	1339	810	370	673	1748	409
B3LYP/6-311+G(d)	1350	809	364	668	1774	411
CCSD(T)/TZ2P[a]	1290	805	371	658	1688	409
CCSD(T)/cc-pVDZ	1342	798	345	640	1801	390
expt[c]	1286	793	370	652	1685	408

[a] Reference 19. [b] Janowski, B.; Knauth, H. D.; Martin, H. *Ber. Bunsun-Ges. Phys. Chem.* **1977**, *81*, 1262. [c] Shimanouchi, T. *J. Phys. Chem. Ref. Data* **1977**, *6*, 993.

32.17 kcal/mol, which is excellent agreement with CCSD(T)/cc-pVTZ//CCSD(T)/cc-pVDZ (31.34 kcal/mol).

A comparison of calculated and measured frequencies of *cis*- and *trans*-ONOCl and $ClNO_2$ is presented in Table 2. The calculated frequencies are in agreement with each other for *cis*-ONOCl with slightly less agreement for the torsion ($\omega_6(a'')$). For $ClNO_2$, the calculated frequencies agreed with each other and are close to the experimental results.

The NO + ClO system studied here is similar to the reaction of XO (X = H, F, Cl) and alkylperoxy radicals (ROO) with NO.[14,44] A negative activation energy is observed for the NO + ClO reaction, which strongly implies the involvement of an ONOCl intermediate.

Computational studies to find a low activation barrier for the ROONO and HOONO unimolecular isomerization have failed.[14,18,44] In the study by Zhao et al.,[14] the transition state for *cis*-HOONO to NO_2 + OH was located 3 kcal/mol above NO_2 + OH radicals at the UCCSD(T)/6-31+G(d)//UCCSD/6-31+G(d) level. In our system, the transition state for *cis*-ONOCl to NO_2 + Cl is found at the RCCSD(T)/cc-pVDZ level. The stationary point has one imaginary frequency and is 1.17 kcal/mol lower than that for NO_2 + Cl at the RCCSD(T)/cc-pVTZ//RCCSD(T)/cc-pVDZ level. The *trans*-ONOCl → $ClNO_2$ reaction has a much higher activation barrier than the cis isomer. The O···Cl distance in the transition state (Figure 2, abst-Cl-ts-t) is much shorter (2.191 Å) than the O···Cl distance in abst-Cl-ts-c (2.939 Å). In addition, the two N−O distances are much more asymmetric in abst-Cl-ts-t compared to abst-Cl-ts-c.

Basically, the abst-Cl-ts-c and abst-Cl-ts-t transition states are indistinguishable from fragmentation into NO_2 + Cl radicals. In their study of the c-HOONO → $HONO_2$ reaction, Dixon et al.[18] located a transition state with an activation energy of 21.4 kcal/mol using MP2/cc-pVTZ where the transition state was 1.6 kcal/mol higher than that for NO_2 + OH. Zhao et al.[14] located a similar transition state at the CBS-QB3 level 21.0 higher than c-HOONO and 2.7 kcal/mol higher than a NO_2/OH complex, but they were unable to say whether the transition state corresponded to fragmentation or isomerization. The N···O distances in the two studies were quite long (2.784 and 3.070 Å at MP2/cc-pVTZ and CBS-QB3, respectively). In contrast to the c-HOONO → $HONO_2$ reaction, the t-ONOF → FNO_2 and t-ONOCl → $ClNO_2$ reactions have much tighter transition states. Ellison el al.[15] calculated a short breaking O···F distance in the t-ONOF → FNO_2 transition state (1.726 and 1.693 Å at RCCSD(T)/pVTZ and UCCSD(T)/pVTZ, respectively) whereas we calculate a 2.191 Å O···Cl distance at RCCSD(T)/cc-pVDZ.

The energy difference between abst-Cl-ts-t and abst-Cl-ts-c is 15.21 kcal/mol at the RCCSD(T)/cc-pVTZ//RCCSD(T)/cc-pVDZ level. The reason for the large activation energy difference can be explained with an explanation similar to that given in the study of O−O cleavage in ONOONO[45] and the mechanism of peroxynitrous acid and methyl peroxynitrite (ROONO).[14] The singly occupied a_1 and doubly occupied b_2 orbitals of NO_2 fragment can mix through the lowering of symmetry from C_{2v} to C_s caused by the approaching Cl radical (Figure 4a). The mixing causes unpaired spin density to reside on the oxygen atoms. The oxygen atom that will form a bond with chlorine has the larger lobe pointing toward the interior angle of the NO_2 fragment. A better overlap between this lobe and the chlorine atom results when the chlorine atom approaches from the cis side compared to the trans side.

The mechanism for O···Cl bond formation in NO_2 + Cl → *trans*-ONOCl (Figure 4b) can be viewed as initial electronic promotion followed by bond formation. The electronic reorganization involves the promotion of a β-spin electron from a b_2 orbital to an a_1 orbital, which leaves an unpaired electron on oxygen in an orbital with significant extent away from the interior angle and suitable for bond formation with a chlorine atom approaching from that direction. Thus, bond formation from the "cis side" of NO_2 requires orbital mixing whereas bond formation from the "trans side" of NO_2 requires electronic promotion. The need for electronic promotion is the source of the greater energy of abst-Cl-ts-t compared to abst-Cl-ts-c. An alternative explanation in term of correlating the reaction path with the $^2A_1$ or $^2B_2$ electronic state of NO_2 is also possible.[14,45]

Rate Calculations

Radical−radical recombinations have long presented experimental and theoretical difficulties.[46−48] The very fast rates require specialized experimental techniques whereas reactions with no activation barriers are difficult to model theoretically. The phase-space-integral based VTST (PSI-VTST) method, as implemented in VariFlex, was used to evaluate the reactive flux as the N−O distances increased from 1.6 to 4.0 Å with a step size 0.1 Å for *cis*-ONOCl and *trans*-ONOCl intermediates. To evaluate the reactive flux accurately, the transition from free rotation to hindered rotation must be treated correctly.

We also used variational transition state theory, as implemented Polyrate, to calculate the rate constant for disappearance (k_{dis}) of reactants (NO + ClO). The reactive flux is calculated at a set of structures optimized at the UB3LYP/6-311+G(d) level with fixed central N−O distances of 3.0, 3.25, 3.50, 3.75, and 4.00 Å. The minimum reactive flux was found at 3.50 Å for *trans*-ONOCl. For *cis*-ONOCl the smallest flux was at 4.00 Å, which we used as the minimum value because we could not compute the rate constant at larger N···O separations.

We also considered the electronic partition function, which was explained in detail in the study of the $O(^3P)$ + OH reaction by Graff and Wagner.[49] The factor was calculated from eq 5

$$p(T)\,k_0(T) = \frac{1}{\sum_j e^{-\epsilon_j/kT}} k_0(T) \qquad (5)$$

where $p(T)$ is the probability that the collision involves the

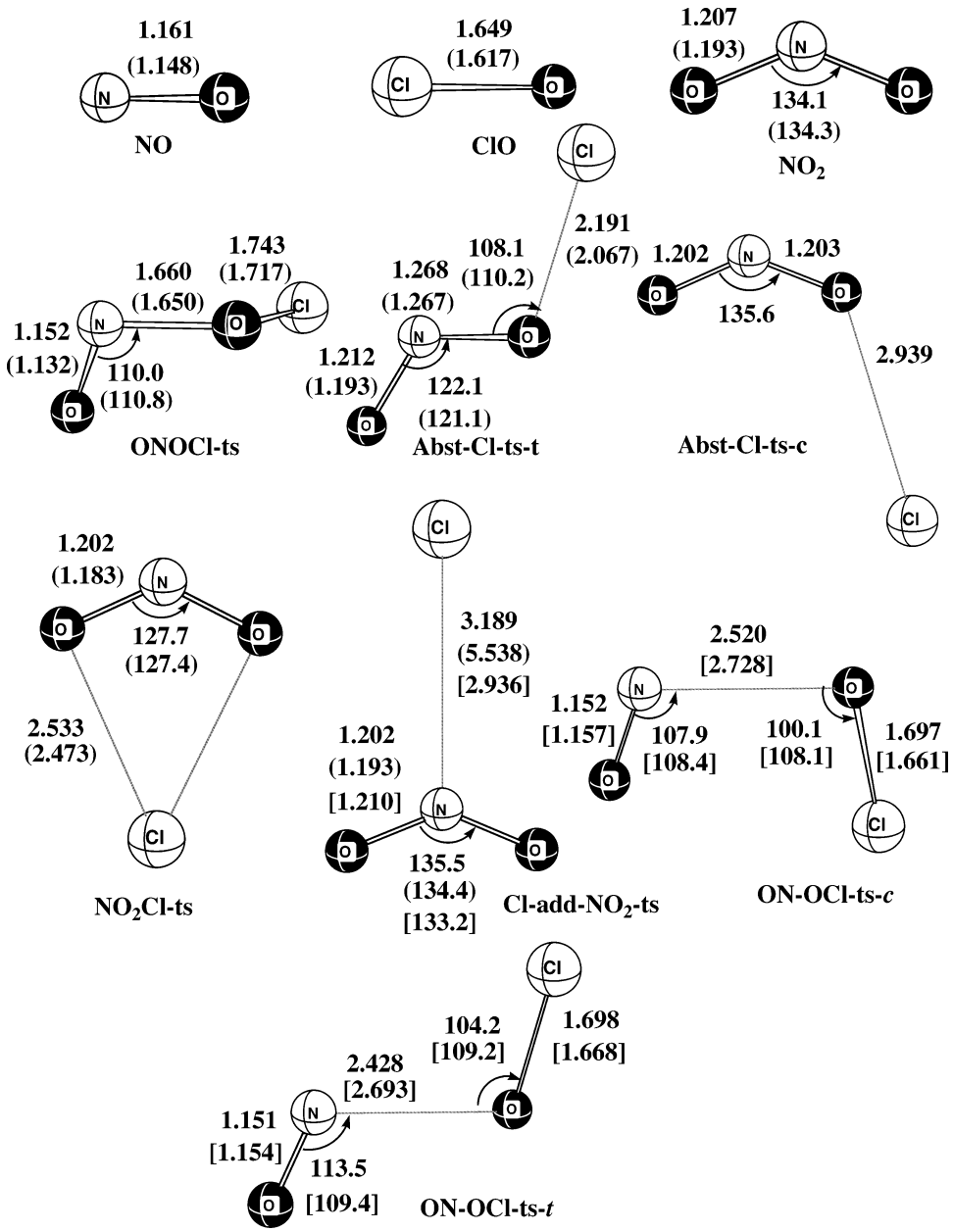

Figure 2. Optimized geometric parameters of stationary points at the CCSD(T)/cc-pVDZ level with B3LYP/6-311+G(d) values in parentheses. Bond lengths are in angstroms and angles are in degrees. The geometric parameters for ON-OCl-ts-c and ON-OCl-ts-t are at the RCCSD(T)/cc-pVDZ level with values at the UCCSD(T)/cc-pVDZ level given in brackets.

"reactive" electronic state and $k_0(T)$ and ϵ_j are the rate constant and the electronic energy (relative to lowest energy) summed over j states. Four singlet states were calculated ($j = 4$, two $^1A'$ and two $^1A''$) at the CASPT2(12,12)/ANO-L level using B3LYP/6-311+G(d) structures at fixed N···O separations (see Table S4 for relative energies of states).

The rate constant for disappearance of reactants (k_{dis}) is the sum of k_1 and k_3 from the mechanism in Scheme 1. The rate constant for formation of products k_{obs} is derived with a steady-state approximation for *cis*- and *trans*-ONOCl

$$k_{obs} = \frac{k_1k_2(k_{-3} + k_4) + k_2k_3k_4}{(k_{-3} + k_4)(k_{-1} + k_2) + k_{-3}k_{-4}}$$

(see derivation in Figure S1 in Supporting Information). The barrier for direct formation of NO_2 + Cl (31.83 kcal/mol) from *trans*-ONOCl is much higher than the barrier for isomerization to *cis*-ONOCl (8.75 kcal/mol). Thus, our mechanism includes direct formation of NO_2 + Cl from *cis*-ONOCl, but isomerization and then fragmentation of *cis*-ONOCl for *trans*-ONOCl.

Figure 5 compares the calculated VariFlex and Polyrate rate constants (high-pressure limit) with experiments and the calculations of Zhu and Lin.[16] Our rate constants are in good agreement with experiment over the temperature range of 200−400 K. Over the temperature range 200−1000 K, we fit our VariFlex rate constant data (k_{obs}) to the form $7.38 \times 10^{-13}T^{0.413}$ exp(286/T) cm^3·molecule^{-1}·s^{-1}. In comparison, the VariFlex rate constant for k_{dis} ($k_1 + k_3$) can be fit to the form $k_{dis} = 3.30 \times 10^{-13}T^{0.558}$ exp(305/T) cm^3·molecule^{-1}·s^{-1}. Before the Polyrate rate constants k_{dis} were computed, the CASPT2 energies (relative to the NO + ClO asymptote) were raised by 1.0 kcal/mol to achieve better agreement with experiment.

The downward (convex) curve of the Zhu and Lin plot reveals non-Arrhenius behavior at high temperature and is due to the negative exponent of temperature in their expression $k_{obs} = 1.43 \times 10^{-9}T^{-0.83}$ exp(92/T) cm^3·molecule-^{1}·s^{-1}. Our plot indicates

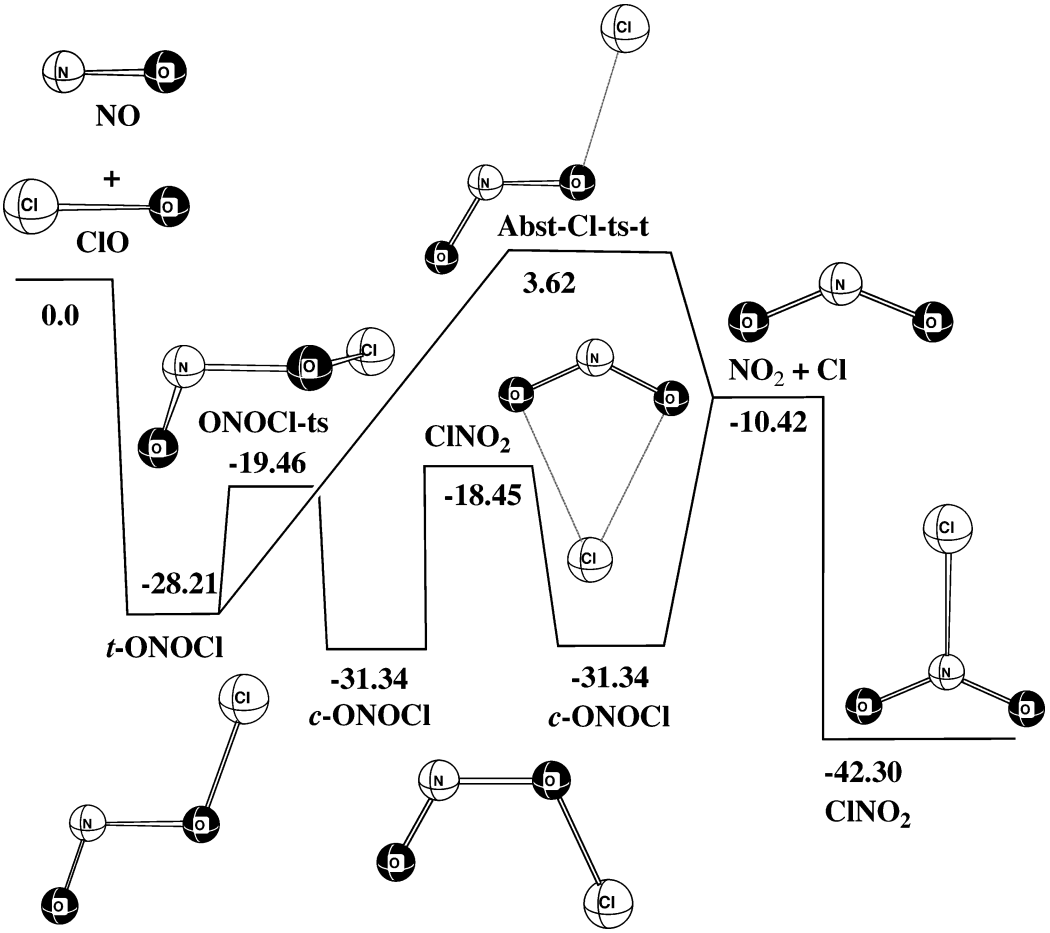

Figure 3. Schematic diagram of the potential energy surface for the NO + ClO system computed at the CCSD(T)/cc-pVTZ//CCSD(T)/cc-pVDZ level. Relative energies are given in kcal/mol at 298 K.

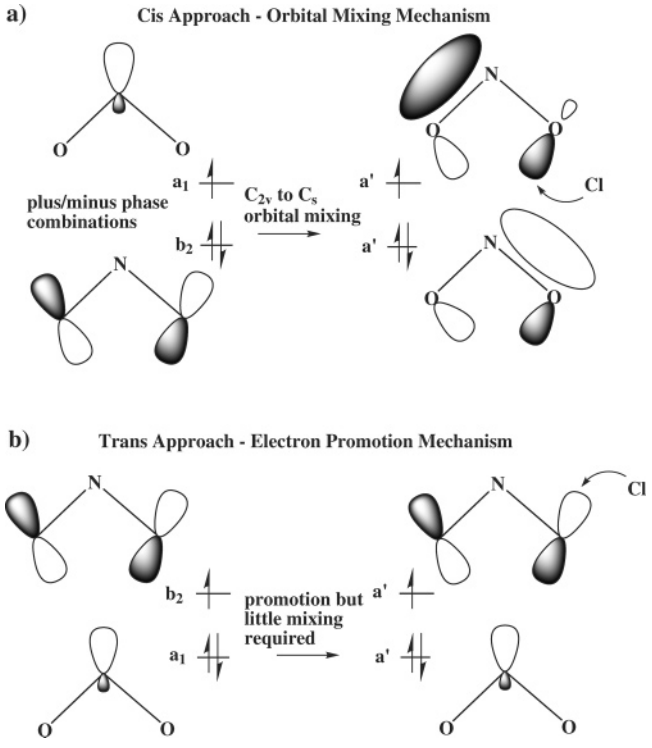

Figure 4. Illustration of cis and trans chlorine addition to NO_2 to form (a) *cis*-ONOCl and (b) *trans*-ONOCl. Cis addition can be rationalized by an orbital mixing mechanism. Trans addition has a higher activation barrier and involves an electron promotion mechanism.

SCHEME 1

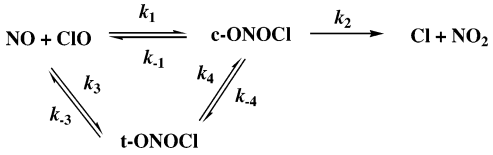

an upward (concave) curve due to the positive exponent of temperature in our rate constant expression $k_{obs} = 7.38 \times 10^{-13}T^{0.413} \exp(286/T)$ cm^3·molecule^{-1}·s^{-1}. The experimental data do not extend to a high enough temperature range to indicate either a concave or convex high-temperature deviation of the rate constant from Arrhenius behavior. We note that both VariFlex and Polyrate indicate a concave curve for k_{dis}.

Generally, nonlinearity in an Arrhenius plot at low temperature is explained by the quantum-mechanical tunneling effect and/or the appearance of an additional reaction channel. However, in our system, there is no tunneling and no competition between two channels. The curvature in the Arrhenius plot at high temperatures can be explained by the excitation of vibrational modes.[50,51] As the population of the excited vibrational modes increase with increasing temperature, the reaction probability increases. Therefore, enhancement of the reactivity causes an increase in reaction rate at high temperatures.

The individual values of k_1 (k_{cis}) and k_3 (k_{trans}) by VariFlex are given in Figure 5 and can be used to compute a cis:trans branching ratio for the initial formation of isomers. At low temperature, the ratio of *cis*-ONOCl is much greater than that of *trans*-ONOCl (1:0.65, 200 K), but the ratio is reduced at high temperature (1:0.83, 500 K).

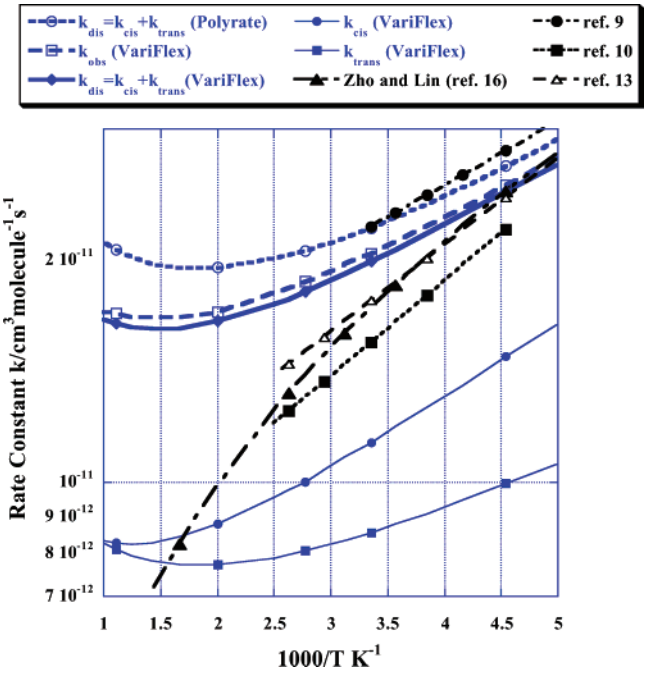

Figure 5. Calculated and experimental rate constants for the ClO + NO reaction. All references are experimental rate data except ref 16, which is computational. The computational rate data are for the bimolecular rate constant at the high-pressure limit. The thin lines for the cis and trans rate constants are added together to give k_{dis}.

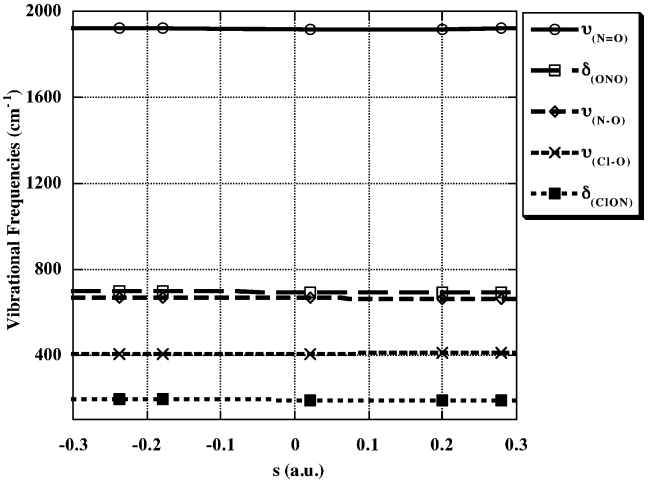

Figure 6. Plot of vibrational frequencies (cm^{-1}) along the IRC for trans → cis isomerization with the reaction projected out. The level of theory is B3LYP/6-311+G(d).

ChemRate and Polyrate were used to calculate the isomerization (*trans*-ONOCl ↔ *cis*-ONOCl) rate constant. ChemRate contains a master equation solver so that rate constants for unimolecular reactions in the energy transfer region and chemical activation processes under steady and non-steady conditions can be determined on the basis of RRKM theory. The input from the electronic structure programs was very similar, except that CCSD(T)/cc-pVTZ//CCSD(T)/cc-pVDZ energies were used in ChemRate and G3B3//B3LYP/6-311+G(d) energies were used in Polyrate.

The vibrational frequencies as a function of *s* for the *trans*-ONOCl → *cis*-ONOCl isomerization reaction are shown in Figure 6 where positive values of *s* correspond to the product side and negative values to the reactant side. The torsion mode is not represented in Figure 6 because it is the imaginary frequency in this range of the reaction coordinate. There is little variation in reaction coordinate, which indicates that these modes do not have a strong contribution to the reaction dynamics.

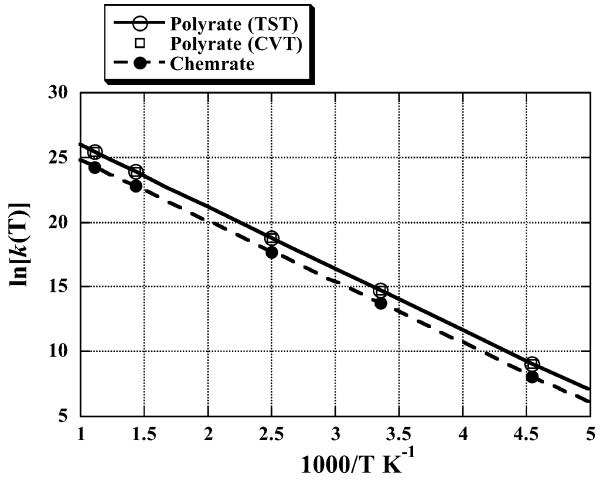

Figure 7. Comparison of ln(k) versus $1/T$ for transition state theory (TST) and variational transition state theory (CVT). The ChemRate results are RRKM.

The Arrhenius plots in Figure 7 show that the TST and CVT curves nearly overlap, which indicates that the variational effect on the calculation of rate constant is very small and can be ignored. The rate constant for trans → cis isomerization ($k_4 = 1.92 \times 10^{13} \exp(-4730/T)$ s^{-1}; Polyrate-TST) is found to obey the Arrhenius equation at 1 atm in the temperature range 200−2000 K.

Conclusion

The NO + ClO → NO_2 + Cl reaction has been a challenge to experiment and theory. This reaction and ones similar to it, such as NO + OH, NO + O_2H, and NO + OF, have been used as a test-bed for computational methods. We have used a series of theoretical methods to elucidate the reaction mechanism. Variational transition state theory was used to compute initial rate constants for the addition reaction to form *cis*- and *trans*-ONOCl. The branching ratio favors the cis isomer at lower temperature (1:0.65 at 200 K). The O···Cl bond fragmentation is predicted to have a significantly different barrier in *cis*-ONOCl (19.75 kcal/mol) compared to *trans*-ONOCl (31.83 kcal/mol). This difference leads to the interesting prediction that the trans isomer must first isomerize to the cis isomer before a chlorine atom leaves. The rate constants for disappearance of reactants (k_{dis}) and appearance of products (k_{obs}) are almost identical and show a pronounced concave curvature indicating non-Arrhenius behavior at higher temperature. Over the temperature range 200−400 K the activation energy is −0.35 kcal/mol (k_{dis}).

Acknowledgment. Computer time was made available on the Alabama Supercomputer Network and the Auburn COSAM PRISM cluster. We thank Dr. Rongshun Zhu from Emory University for helpful conversations. Dr. David Stanbury provided help with the kinetic derivation.

Supporting Information Available: CCSD(T)/cc-pVDZ and CCSD(T)/cc-pVTZ//CCSD(T)/cc-pVTZ energies (hartrees), zero-point energies (kcal/mol), heat capacity corrections to 298K (kcal/mol), entropies (cal/mol·K) at the CCSD(T)/cc-pVDZ and B3LYP/6-311+G(d) level are tabulated in Table S1. Relative CASPT2(12,12)/ANO-L//B3LYP/6-311+G(d) electronic energies, Polyrate rate constant results, the electronic partition factor, and rate constants in Scheme 1 (k_1-k_4) are given in support

information Tables S2-S5, respectively. Cartesian coordinates of all optimized structures at the RCCSD(T)/cc-pVDZ (and several at UCCSD(T)/cc-pVDZ) level of theory are given in Table S6. A derivation of the kinetic expression for formation of products (k_{obs}) is given in Figure S1. This material is available free of charge via the Internet at http://pubs.acs.org.

References and Notes

(1) Wofsy, S. C.; McElroy, M. B. *Can. J. Chem.* **1974**, *52*, 1582.

(2) Farman, J. C.; Gardiner, B. G.; Shanklin, J. D. *Nature* **1985**, *315*, 207.

(3) Stolarski, R. S.; Cicerone, R. J. *Can. J. Chem.* **1974**, *52*, 1610.

(4) Brune, W. H.; Toohey, D. W.; Anderson, J. G.; Chan, K. R. *Geophys. Res. Lett.* **1990**, *17*, 505.

(5) Waters, J. W.; Froidevaux, L.; Read, W. G.; Manney, G. L.; Elson, L. S.; Flower, D. A.; Jarnot, R. F.; Harwood, R. S. *Nature* **1993**, *362*, 597.

(6) Fickert, S.; Helleis, F.; Adams, J. W.; Moortgat, G. K.; Crowley, J. N. *J. Phys. Chem.* A **1998**, *102*, 10689.

(7) Carter, R. T.; Hallou, A.; Huber, J. R. *Chem. Phys. Lett.* **1999**, *310*, 166.

(8) Clyne, M. A. A.; Watson, R. T. *J. Chem. Soc., Faraday Trans.* **1974**, *70*, 2250.

(9) Zahniser, M. S.; Kaufman, F. *J. Chem. Phys.* **1977**, *66*, 3673.

(10) Leu, M. T.; DeMore, W. B. *J. Phys. Chem.* **1978**, *82*, 2049.

(11) Clyne, M. A. A.; MacRobert, A. J. *Int. J. Chem. Kinet.* **1980**, *12*, 79.

(12) Ray, G. W.; Watson, R. T. *J. Phys. Chem.* **1981**, *85*, 2955.

(13) Lee, Y.-P.; Stimpfle, R. M.; Perry, R. A.; Mucha, J. A.; Evenson, K. M.; Jennings, D. A.; Howard, C. J. *Int. J. Chem. Kinet.* **1982**, *14*, 711.

(14) Zhao, Y.; Houk, K. N.; Olson, L. P. *J. Phys. Chem. A* **2004**, *108*, 5864.

(15) Ellison, G. B.; Herbert, J. M.; McCoy, A. B.; Stanton, J. F.; Szalay, P. G. *J. Phys. Chem. A* **2004,** *108*, 7639.

(16) Zhu, R. S.; Lin, M. C. *Chem. Phys. Chem.* **2004**, *5*, 1.

(17) Bach, R. D.; Dmitrenko, O.; Estévez, C. M. *J. Am. Chem. Soc.* **2003**, *125*, 16204.

(18) Dixon, D. A.; Feller, D.; Zhan, C.-G.; Francisco, J. S. *J. Phys. Chem. A* **2002**, *106*, 3191.

(19) Lee, T. J.; Bauschlicher, C. W.; Jayatilaka, D. *Theor. Chem. Acc.* **1997**, *97*, 185.

(20) Guha, S.; Francisco, J. S. *J. Phys. Chem. A* **1997**, *101*, 5347.

(21) Francisco, J. S.; Clark, J. *J. Phys. Chem. A* **1998**, *102*, 2209.

(22) Parthiban, S.; Lee, T. J. *J. Chem. Phys.* **2000**, *113*, 145.

(23) Lee, T. J.; Scuseria, G. E. *J. Chem. Phys.* **1990**, *93*, 489.

(24) Scuseria, G. E. *J. Chem. Phys.* **1991**, *94*, 442.

(25) Frisch, M. J.; Trucks, G. W.; Schlegel, H. B.; Scuseria, G. E.; Robb, M. A.; Cheeseman, J. R.; Montgomery, J. A., Jr.; Vreven, T.; Kudin, K. N.; Burant, J. C.; Millam, J. M.; Iyengar, S. S.; Tomasi, J.; Barone, V.; Mennucci, B.; Cossi, M.; Scalmani, G.; Rega, N.; Petersson, G. A.; Nakatsuji, H.; Hada, M.; Ehara, M.; Toyota, K.; Fukuda, R.; Hasegawa, J.; Ishida, M.; Nakajima, T.; Honda, Y.; Kitao, O.; Nakai, H.; Klene, M.; Li, X.; Knox, J. E.; Hratchian, H. P.; Cross, J. B.; Adamo, C.; Jaramillo, J.; Gomperts, R.; Stratmann, R. E.; Yazyev, O.; Austin, A. J.; Cammi, R.; Pomelli, C.; Ochterski, J. W.; Ayala, P. Y.; Morokuma, K.; Voth, G. A.; Salvador, P.; Dannenberg, J. J.; Zakrzewski, V. G.; Dapprich, S.; Daniels, A. D.; Strain, M. C.; Farkas, O.; Malick, D. K.; Rabuck, A. D.; Raghavachari, K.; Foresman, J. B.; Ortiz, J. V.; Cui, Q.; Baboul, A. G.; Clifford, S.; Cioslowski, J.; Stefanov, B. B.; Liu, G.; Liashenko, A.; Piskorz, P.; Komaromi, I.; Martin, R. L.; Fox, D. J.; Keith, T.; Al-Laham, M. A.; Peng, C. Y.; Nanayakkara, A.; Challacombe, M.; Gill, P. M. W.; Johnson, B.; Chen, W.; Wong, M. W.; Gonzalez, C.; Pople, J. A. *Gaussian03*, Revision B.4; Gaussian, Inc.: Pittsburgh, PA, 2003.

(26) Karlström, G.; Lindh, R.; Malmqvist, P.-Å.; Roos, B. O.; Ryde, U.; Veryazov, V.; Widmark, P.-O.; Cossi, M.; Schimmelpfennig, B.; Neogrady, P.; Seijo, L. *Comput. Mater. Sci.* **2003**, *28*, 222.

(27) Schaftenaar, G.; Noordik, J. H. *J. Comput.-Aided Mol. Design* **2000**, *14*, 123.

(28) Woon, D. E.; Dunning, T. H. *J. Chem. Phys.* **1993**, *98*, 1358.

(29) Kendall, R. A.; Dunning, T. H.; Harrison, R. J. *J. Chem. Phys.* **1994**, *100*, 7410.

(30) Curtiss, L. A.; Raghavachari, K.; Redfern, P. C.; Rassolov, V.; Pople, J. A. *J. Chem. Phys.* **1998**, *109*, 7764.

(31) Moore, C. E. *Atomic Energy Levels*; NSRDS-NBS 35; National Bureau of Standards: Washington, DC, 1971; Vols. II and II.

(32) Coxon, J. A. *Can. J. Phys.* **1979**, *57*, 1538.

(33) Sayin, H.; McKee, M. L. *J. Phys. Chem. A* **2004**, *108*, 7613.

(34) The standard G3B3 method includes spin−orbit corrections for atoms but not for diatomic molecules. We have included spin−orbit effects for NO and ClO in the G3B3 energies.

(35) Roos, B. O. The complete active space self-consistent field method and its applications in electronic structure calculations. In *Advances in Chemical Physics; Ab Initio Methods in Quantum Chemistry-II*; Lawley, K. P., Ed.; John Wiley & Sons: Chichester, U.K., 1987.

(36) (a) Roos, B. O.; Andersson, K.; Fülscher, M. P.; Malmqvist, P.-Å.; Serrano-Andrés, L.; Pierloot, K.; Merchán, M. Multiconfigurational perturbation theory: Applications in electronic spectroscopy. In *Advances in Chemical Physics: New Methods in Computational Quantum Mechanics*; Prigogine, I., Rice, S. A., Eds.; John Wiley & Sons: New York, 1995. (b) Andersson, K.; Malmqvist, P.-Å.; Roos, B. O.; Sadlej, A. J.; Wolinski, K. *J. Phys. Chem.* **1990**, *94*, 5483. (c) Andersson, K.; Malmqvist, P.-Å.; Roos, B. O. *J. Phys. Chem.* **1992**, *96*, 1218.

(37) (a) Widmark, P. O.; Malmqvist, P.-Å.; Roos, B. O. *Theor. Chim. Acta* **1990**, *77*, 291. (b) Widmark, P. O.; Malmqvist, P.-Å.; Roos, B. O. *Theor. Chim. Acta* **1991**, *79*, 419.

(38) Corchado, J. C.; Chuang, Y.-Y.; Fast, P. L.; Villa, J.; Hu, W.-P.; Liu, Y.-P.; Lynch, G. C.; Nguyen, K. A.; Jackels, C. F.; Melissas, V. S.; Lynch, I. R.; Coitino, E. L.; Fernandez-Ramos, A.; Pu, J.; Albu, T. V.; Steckler, R.; Garrett, B. C.; Isaacson, A. D.; Truhlar, D. G. Polyrate, Version 9.3, University of Minnesota, 2004.

(39) Klippenstein, S. J.; Wagner A. F.; Dunbar, R. C.; Wardlaw, D. M.; Robertson, S. H. VariFlex, Version 1.00; Argonne National Laboratory: Argonne, IL, 1999.

(40) Mokrushin, V.; Bedanov, V.; Tsang, W.; Zachariah, M. R.; Knyazev, V. D. ChemRate, Version 1.19; National Institute of Standards and Technology: Gaithersburg, MD, 2002.

(41) Tevault, D. E.; Smardzewski, R. R. *J. Chem. Phys.* **1977**, *67*, 3777.

(42) Kawashima, Y.; Takeo, H.; Matsumura, C. *Chem. Phys. Lett.* **1979**, *63*, 119.

(43) The NIST Standard Reference Database (http://webbook.nist.gov/chemistry) was used as the source of all thermochemistry.

(44) Zhang, D.; Zhang, R.; Park, J.; North, S. W. *J. Am. Chem. Soc.* **2002**, *124*, 9600.

(45) Olson, L. P.; Kuwata, K. T.; Bartberger, M. D.; Houk, K. N. *J. Am. Chem. Soc.* **2002**, *124*, 9469.

(46) Slagle, I. R.; Gutman D.; Davies, J. W.; Pilling, M. J. *J. Phys. Chem.* **1988**, *92*, 2455.

(47) Song, S.; Hanson, R. K.; Bowman, C. T.; Golden, D. M. *J. Phys. Chem. A* **2002**, *106*, 9233.

(48) Miller, J. A.; Klippenstein, S. J. *J. Phys. Chem.* A **2000**, *104*, 2061.

(49) Graff, M. M.; Wagner, A. F. *J. Chem. Phys.* **1990**, *92*, 2423.

(50) Kandel, S. A.; Zare, R. N. *J. Chem. Phys.* **1998**, *109*, 9719.

(51) Michelsen, H. A. *Acc. Chem. Res.* **2001**, *34*, 331.

(52) Millen, D. J.; Sinnot, K. M. *J. Chem. Soc.* **1958**, 350.